Biological Cybernetics (2018) 112:305–321
https://doi.org/10.1007/s00422-018-0752-3

Biological Cybernetics

ORIGINAL ARTICLE

The role of long-range coupling in crayfish swimmeret phase-locking

Lucy E. Spardy[1] · Timothy J. Lewis[2]

Received: 13 April 2017 / Accepted: 23 February 2018 / Published online: 22 March 2018

Abstract
During forward swimming, crayfish and other long-tailed crustaceans rhythmically move four pairs of limbs called swimmerets to propel themselves through the water. This behavior is characterized by a particular stroke pattern in which the most posterior limb pair leads the rhythmic cycle and adjacent swimmerets paddle sequentially with a delay of roughly 25% of the period. The neural circuit underlying limb coordination consists of a chain of local modules, each of which controls a pair of limbs. All modules are directly coupled to one another, but the inter-module coupling strengths decrease with the distance of the connection. Prior modeling studies of the swimmeret neural circuit have included only the dominant nearest-neighbor coupling. Here, we investigate the potential modulatory role of long-range connections between modules. Numerical simulations and analytical arguments show that these connections cause decreases in the phase-differences between neighboring modules. Combined with previous results from a computational fluid dynamics model, we posit that this phenomenon might ensure that the resultant limb coordination lies within a range where propulsion is optimal. To further assess the effects of long-range coupling, we modify the model to reflect an experimental preparation where synaptic transmission from a middle module is blocked, and we generate predictions for the phase-locking properties in this system.

Keywords Phase-locking · Synchronization · Phase-wave · Central pattern generator · Half-center oscillator · Metachronal wave · Locomotor control · Long-tail crustacean · Perturbation analysis · Limb coordination · Locomotion

1 Introduction

Efficient limbed locomotion results from motor patterns that preserve particular phase relationships between limbs. In various studies of invertebrate systems, it has been shown that the basic motor pattern controlling locomotor movements can be produced by CPGs (pattern-generating circuits in the central nervous system) or networks of CPGs (Hughes and Wiersma 1960; Marder and Bucher 2001). Thus, the neural mechanisms that underlie complex locomotor behavior can be assessed by examining how intrinsic neuronal properties and network connectivity combine to generate and coordinate rhythmic activity in these circuits.

Forward swimming of crayfish provides an example of robust coordinated limb activity. During this behavior, limbs called swimmerets generate thrust by paddling rhythmically with alternating power and return strokes. These limbs occur in four bilateral pairs that are aligned along the abdomen of the segmental body of the crayfish. The swimmerets within each pair move synchronously, but the activation of limb pairs occurs in a back-to-front metachronal wave. The most posterior limb pair begins the cycle and is followed by the sequential activation of neighboring limb pairs, which are delayed by approximately 25% of the overall period. This distinct coordinated limb movement is robust; it is maintained over a large range of swimming frequencies [less than 0.5 to greater than 6 Hz (Mulloney et al. 2006)] and is preserved over the full range of body sizes of crayfish. Furthermore, this phenomenon generalizes beyond the crayfish to other long-tailed crustaceans (Laverack et al. 1976). The swimmeret system rarely exhibits any other behavior.

The crayfish swimmeret system is ideal for studying the neural mechanisms of coordinated motor behavior for sev-

Communicated by J. Leo van Hemmen.

✉ Lucy E. Spardy
lspardy@skidmore.edu

Timothy J. Lewis
tjlewis@ucdavis.edu

[1] Department of Mathematics, Skidmore College, 815 North Broadway, Saratoga Springs, NY 12866, USA

[2] Department of Mathematics, University of California, One Shields Ave, Davis, CA 95616, USA

eral reasons: (1) The system generates the metachronal wave with 25% inter-limb phase-differences almost exclusively, as described above, (2) the isolated ventral nerve cord is capable of producing this pattern without the influence of sensory feedback, and thus the behavior can be examined by studying the neural circuitry alone, and (3) the neural circuitry that produces this behavior has been well characterized and is made up of a relatively small number of neurons and interconnecting axons (Mulloney and Smarandache-Wellmann 2012). The circuit is comprised of a series of interconnected local modules (CPGs) in which the pattern-generating kernel is a half-center oscillator (HCO). Each module can independently produce the rhythmic motor output that drives a corresponding limb. Connections between the oscillating modules adjust the phases of activity to produce the observed coordinated metachronal behavior.

Previous studies have modeled the segmented neural circuit of the crayfish swimmeret system as a chain of coupled oscillators. This body of work explored the capabilities of various connection topologies and suggested conditions necessary to generate the back-to-front progression with 25% phase-differences that characterize the swimming stroke pattern (Skinner et al. 1997; Jones et al. 2003; Jones and Kopell 2006). More recently, Zhang et al. incorporated current knowledge of the network connectivity and concluded that the circuit architecture provides a robust mechanism for metachronal swimming (Zhang et al. 2014; Zhang and Lewis 2016). All of these models have represented the circuitry with coupling between nearest-neighbor oscillators only. However, longer-range connections exist. The strengths of these connections are weaker than those between nearest-neighbors (Smarandache et al. 2009), but they have the ability to coordinate activity when a middle oscillating module is blocked (Tschuluun et al. 2001). These results suggest that the long-range connections may play a functional role in coordinating limb movements of the swimmerets.

Here, we consider the effects of long-range coupling on coordination in chains of oscillators that capture known features of the crayfish swimmeret neural circuit. First, we perform numerical simulations of both a conductance-based model and a phase model of a chain of half-center oscillators with long-range connections and examine the effect of varying the strength of long-range connections in these two models. In both cases, we show that the addition of next-nearest-neighbor coupling decreases the phase-differences between neighboring oscillators, thus speeding up the back-to-front metachronal wave of limb paddling. To explain the nature of this phenomenon, we use a perturbation analysis of the phase model to derive expressions that describe how long-range coupling and the phase response properties of the oscillators combine to influence phase-locking in the swimmeret system. We show that the necessary conditions for decreases in phase-differences due to the presence of next-nearest-neighbor coupling appear to be met generically by the crayfish swimmeret neural circuit. Finally, we probe the system further by examining the circuit's behavior when a middle oscillator is blocked, as in experimental studies (Tschuluun et al. 2001). Our results generate phase-locking predictions that depend on the relative ratio of two key parameters that correspond to the strength of the long-range coupling and the phase response properties of the oscillators. Our main focus is to understand the role of the next-nearest-neighbor connections (which we will often refer to simply as *long-range connections*), and in the main text, we largely ignore the effects of the significantly weaker next-next-nearest-neighbor coupling (which we refer to as *longest-range connections*). However, we address the contribution of these longest-range connections in "Appendix B."

2 Long-range connections decrease phase-differences between neighboring limbs

2.1 The swimmeret neural circuit as a chain of half-center oscillators (HCOs)

The coordinated movements of crayfish swimmerets are driven by a motor pattern that is generated by a neural circuit within its central nervous system. This system is segmented into four distinct ganglia, each of which contains two neural modules. Each module includes a pattern-generating kernel, a set of coordinating neurons, and a set of motor neurons that constitutes the complete motor innervation of an individual swimmeret (Mulloney and Smarandache 2010). Thus, the swimmeret neural circuit is a chain of four interconnected local sub-circuits. The circuit is shown schematically in Fig. 1a. Note that the diagram only depicts the circuit for one side of the crayfish's body.

The pattern-generating kernel of each module is formed by nonspiking local interneurons, IPS neurons (inhibitors of power stroke), and IRS neurons (inhibitors of return stroke) (Smarandache-Wellmann et al. 2013) that are connected by reciprocal inhibition. This "half-center" structure generates robust antiphase oscillations that are responsible for the coordination of the power and return stroke motor neurons. These antiphase oscillations are intrinsic to the local half-center oscillator (HCO), i.e., activation of the oscillations does not rely on the intersegmental coupling or proprioceptive feedback. Moreover, while the intrinsic frequencies of the HCOs can vary widely, the intrinsic frequencies of the oscillators are not significantly different from one another (Paul and Mulloney 1986; Mulloney 1997).

Activity in the HCO kernels drive spiking neurons, ASC and DSC, whose axons project in the anterior and posterior directions, respectively. The ASC neurons fire bursts

of spikes that are in-phase with the activity of their corresponding module's power stroke motor neurons, and the DSC neurons fire bursts of spikes that are in-phase with activity of the module's return stroke motor neurons (Mulloney et al. 2006). The ASC and DSC neurons reliably encode information about the phase, duty cycle, and strength of their presynaptic partners (Mulloney et al. 2006). Ascending and descending intersegmental input arriving at each module is transmitted to a local nonspiking interneuron, ComInt1 (C1). C1 then transfers the input to the IRS component of the HCO. While the filtering processes of C1 have not been fully explored, preliminary studies suggest that it is well described by a linear process (Smarandache-Wellmann et al. 2014).

All modules in the neural circuit are coupled with one another. The intersegmental coupling in the ascending and descending directions is approximately equal, but the coupling strength substantially weakens with distance between modules. EPSPs from axons originating in next-nearest-neighbors have strengths between 10 and 40% of the strength of EPSPs from axons generated from neighbors, and next-next-nearest-neighbors have exhibited EPSP strengths at 10–15% of those between neighbors (Smarandache et al. 2009).

In summary, the crayfish swimmeret neural circuit is comprised of a chain of HCOs in which there is asymmetry in the ascending and descending connection topology and a decrease in coupling strength with distance between the HCOs. Note that the HCOs are coupled to each other by a sequence of three synaptic connections: Information travels from one HCO to a coordinating neuron (ASC or DSC) and then to a C1 interneuron which in turn projects onto the next HCO. However, because the ASC and DSC neurons provide reliable information about the timing and duration of HCO activity, and because C1 seems not to strongly influence information in the signal it receives, this trisynaptic connection can be modeled as a monosynaptic connection, and therefore the HCOs can be modeled as being directly connected to one another as in Fig. 1b. Indeed, we will model the swimmeret system using this configuration, and we will include the property that the connectivity strength decreases with distance by appropriately scaling the longer range coupling strengths.

2.2 Phase-locking in a conductance-based model of the swimmeret neural circuit

As an initial exploration of the effects of long-range coupling on intersegmental limb coordination, we use the network architecture and assumptions outlined in Sect. 2.1 and Fig. 1b to construct a conductance-based model of (one side of) the swimmeret neural circuit. The intrinsic dynamics of the HCOs are described by the Wang–Rinzel model (Wang and Rinzel 1992). Each HCO consists of two "cells": a P cell and an R cell. The ionic currents in the P and R cells include a rapidly-activating slowly-inactivating inward "post-inhibitory rebound" current and a voltage-independent leakage current. Note that the cells in the HCOs of the swimmeret circuit are nonspiking, and therefore ionic currents that underlie fast spikes are not present in the model. The strong reciprocal inhibitory synapses between cells in each HCO are modeled as "fast threshold modulation" synapses (Somers and Kopell 1993). The cells in the HCOs are nonoscillatory when isolated. However, when coupled through reciprocal inhibition, alternating oscillations with a duty cycle of approximately one half are generated via post-inhibitory rebound (Perkel and Mulloney 1974). The intersegmental connections, i.e., the coupling between the HCOs, are also modeled as "fast threshold modulation" synapses. The synaptic strengths of next-nearest-neighbor connections are scaled by the parameter β to reflect their strength, which is weak relative to synaptic strengths between neighboring HCOs. Details of the conductance-based model are provided in "Appendix A."

We define $0 \leq \phi_j < 1$ to be the intersegmental phase-difference between the $j+1$th and jth HCO. For the conductance-based model, we compute ϕ_j by measuring the difference between times of peak activity in the P cells of the $j+1$th and jth HCO and normalize this by the period of the oscillations.

Figure 2a, b shows the P cell activity for model simulations with nearest-neighbor coupling alone ($\beta = 0$) and with both nearest-neighbor and next-nearest-neighbor coupling ($\beta = 0.3$), respectively. In both cases, activation of power stroke neurons occurs sequentially from the most posterior HCO to the most anterior HCO with roughly 25% phase-differences between HCOs. In the simulation with nearest-neighbor coupling alone, the intersegmental differences are $(\phi_1, \phi_2, \phi_3) = (0.302, 0.313, 0.272)$. When long-range coupling is incorporated, the intersegmental phase-differences in the simulation are $(\phi_1, \phi_2, \phi_3) = (0.239, 0.196, 0.240)$. That is, the intersegmental phase-differences in the network that includes next-nearest-neighbor coupling are significantly smaller than those in the network with nearest-neighbor coupling alone. In fact, Fig. 2c shows that the intersegmental phase-differences tend to decrease as the relative next-nearest-neighbor coupling strength (β) increases well beyond the biophysically realistic range of next-nearest-neighbor coupling strengths.

2.3 Phase model of the swimmeret neural circuitry

The simulation results for the conductance-based model show that in a chain of asymmetrically connected Wang–Rinzel HCOs, long-range connections cause decreases in the phase-differences between neighboring HCOs. In this section, we use an analytically tractable phase model that captures the essential properties of the internal HCO structure and the inter-HCO connectivity to determine the explicit

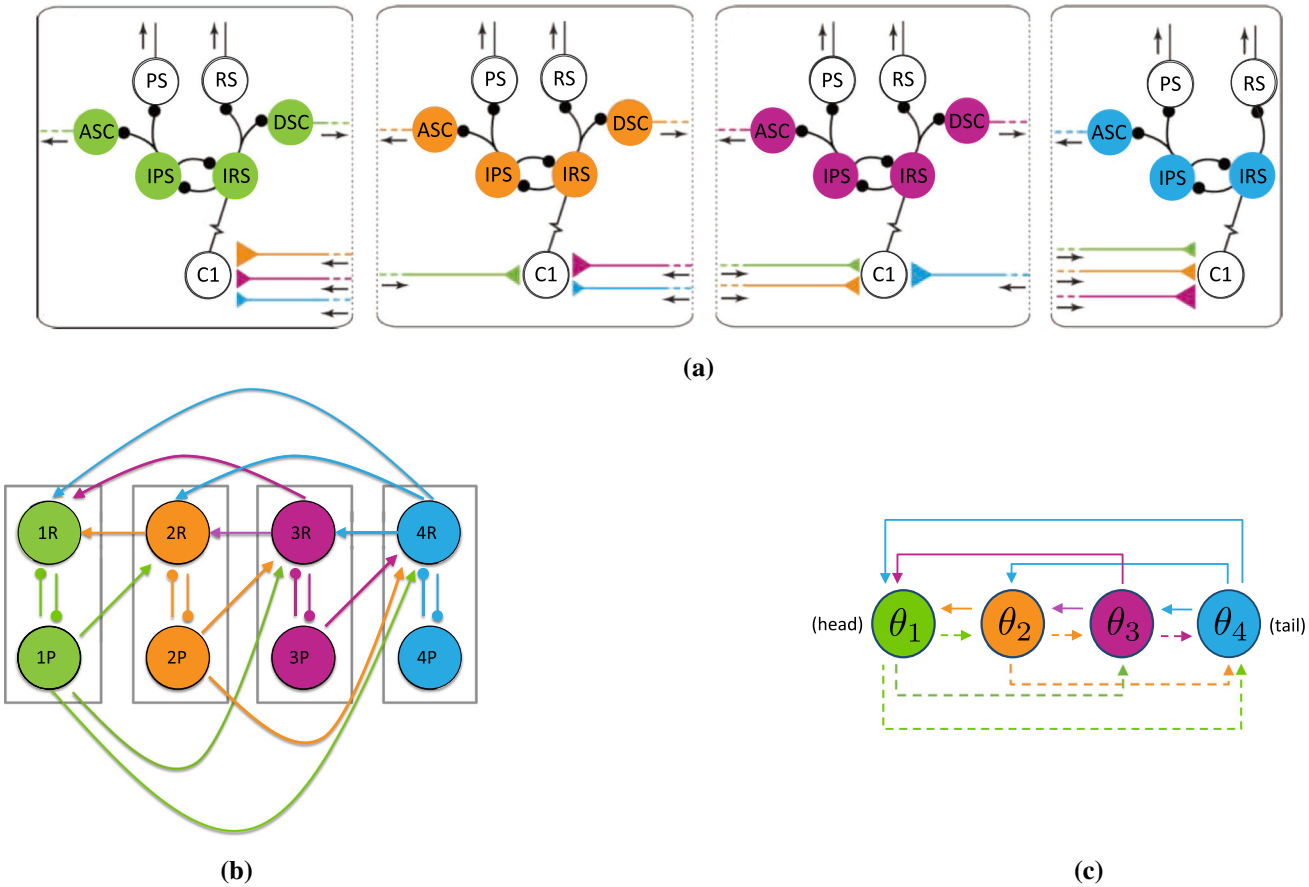

Fig. 1 Neural circuitry responsible for coordination in the crayfish swimmeret system. The system is modular, with each swimmeret controlled by a distinct local pattern generator. Note that the diagrams represent the circuitry innervating swimmerets on one side of the crayfish's body. **a** The circuit is composed of four interconnected local modules in a chain of segmental ganglia. IPS and IRS neurons in each module form a half-center oscillator (HCO) and project in the ascending and descending directions through coordinating neurons, ASC and DSC. Intersegmental input is assimilated within C1 neurons. The connections to C1 are color coordinated to correspond with each presynaptic module. Relative synaptic strength is indicated by triangle size—neighboring coupling strengths are significantly stronger than longer-range connections. **b** Effective configuration of the neural circuitry. A chain of HCOs with asymmetric ascending and descending coupling. *P* and *R* neurons represent units that are in-phase with the power and return strokes, respectively. **c** Phase model representation. Each node tracks the activity of a particular HCO and hence the corresponding activity of the neurons within each local module (i.e., ganglion). To represent the fact that ascending and descending connections come from distinct origins within the local HCO (see **a** and **b**), the phase of the descending input is shifted by half of the period relative to ascending input, i.e., ascending connections with phase θ_j are shown as solid lines, whereas the descending connections have phase $\theta_j + 0.5$, indicated with dashed lines. Figure **a** adapted from Smarandache-Wellmann and Grätsch (2014) (color figure online)

conditions necessary for this phenomenon. [Note that the conductance-based model can be systematically reduced to the phase model in the limit of weak inter-HCO connectivity (Schwemmer and Lewis 2012).]

2.3.1 Description of the phase model

Neural circuits consisting of interconnected CPGs have been often modeled mathematically as chains of coupled phase oscillators, for example, Cohen et al. (1992), Williams et al. (1990), and Skinner et al. (1997). In phase models, the state of the kth oscillator is described completely by its phase $\theta_k \in [0, 1)$. In isolation, the phase θ_k evolves according to some constant intrinsic frequency. The inputs coming from other units can speed up or slow down the oscillators, depending on the structure of the synaptic input, the phase at which it is received, and the oscillators' response properties. These effects are captured by *interaction functions*, which quantify the magnitude of acceleration or deceleration as a function of the phase-difference between the coupled oscillators.

To represent the neural circuit of the crayfish swimmeret system, we augment the phase model described in Zhang et al. (2014) by including long-range coupling,

$$\begin{aligned}
\dot{\theta_1} &= \omega + H_A(\theta_2 - \theta_1) + \beta H_A(\theta_3 - \theta_1)\\
\dot{\theta_2} &= \omega + H_D(\theta_1 - \theta_2) + H_A(\theta_3 - \theta_2) + \beta H_A(\theta_4 - \theta_2)\\
\dot{\theta_3} &= \omega + H_D(\theta_2 - \theta_3) + H_A(\theta_4 - \theta_3) + \beta H_D(\theta_1 - \theta_3)\\
\dot{\theta_4} &= \omega + H_D(\theta_3 - \theta_4) + \beta H_D(\theta_2 - \theta_4). \qquad (1)
\end{aligned}$$

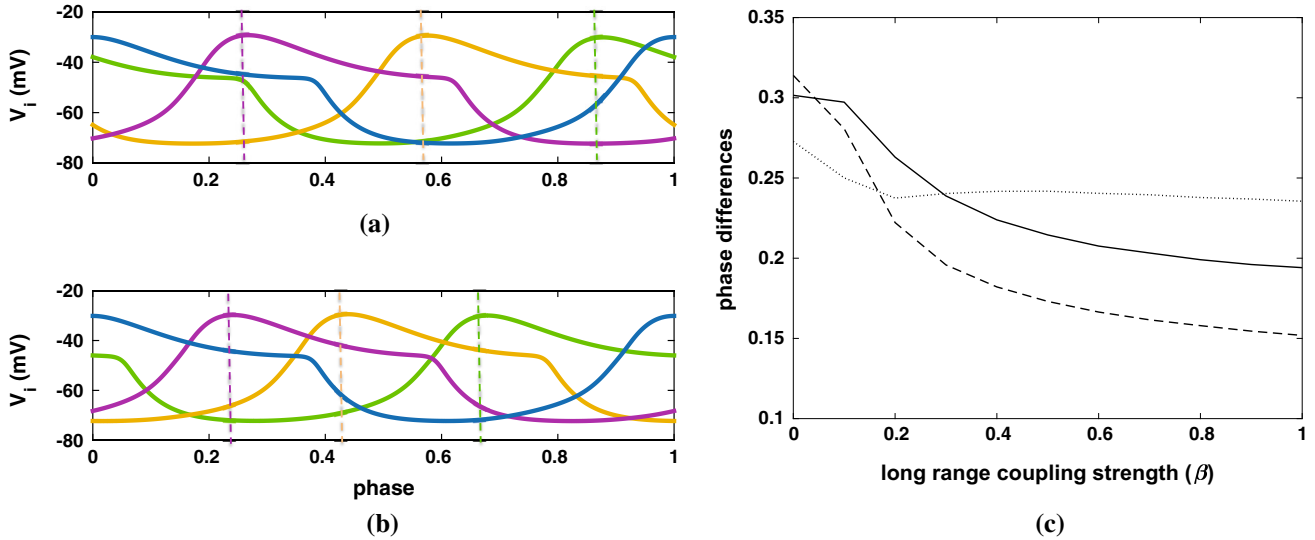

Fig. 2 Numerical simulations for the chain of Wang–Rinzel HCOs with asymmetric coupling. **a** Time course of power stroke neuronal activity for the network with nearest-neighbor intersegmental coupling only. Blue, magenta, gold, and green curves correspond to activity in the fourth, third, second, and first HCOs, respectively (i.e., colors of the curves correspond to the module color in Fig. 1). **b** Neuronal activity when both nearest-neighbor and long-range connections are present. Long-range synaptic strength was chosen to be 30% of the nearest-neighbor strength ($\beta = 0.3$). Line color and style correspond to (**a**). The phase-differences are smaller than in the nearest-neighbor simulation, see text for details. **c** Phase-differences decrease as the long-range coupling strength increases from 0 to 100% of the nearest-neighbor strength ($\beta \in [0, 1]$). Phase-differences ϕ_1, ϕ_2, ϕ_3 shown with solid, dashed, and dotted lines, respectively (color figure online)

Because the isolated swimmeret CPGs have similar frequencies (Paul and Mulloney 1986), the intrinsic frequencies of the oscillators are modeled by a common parameter, ω. The interaction functions H_A and H_D represent the effects in response to inputs from ascending and descending connections, respectively. The outputs of an oscillator in the ascending and descending directions emanate from distinct subunits of each HCO, as shown in Fig. 1a, b, and are out of phase with each other by half of the period. Other than this, the outputs are very similar (Smarandache-Wellmann et al. 2013). We can capture this feature of the circuit by shifting the phase of the descending output by 0.5 relative to the phase of the ascending output (Zhang et al. 2014). That is, we can define the phase of the ascending and descending outputs of the oscillator j to be θ_j and $\theta_j + 0.5$, respectively. Then, if we set the interaction function for an ascending connection from oscillator k to oscillator j to be $H(\theta_k - \theta_j) = H_A(\theta_k - \theta_j)$, the interaction function for a descending connection from oscillator i to oscillator j can be written as

$$H_D(\theta_i - \theta_j) = H(\theta_i + 0.5 - \theta_j) = H(\theta_i - \theta_j + 0.5).$$

The next-nearest-neighbors interaction functions are scaled by the parameter β to reflect the fact that these connections are weak relative to the nearest-neighbor connections. The nearest-neighbor coupling strength is absorbed into the amplitude of the interaction functions. As mentioned earlier, experimental measurements indicate that the next-nearest-neighbors coupling strength is $\beta \sim 0.1 - 0.4$. However, to get a more complete picture of the effects of this long-range coupling, we will vary β between 0 and 1 in simulations of the phase model. $\beta = 0$ corresponds to the case of nearest-neighbor connectivity alone, whereas $\beta = 1$ corresponds to the case where the next-nearest-neighbor and nearest-neighbor coupling strengths are of equal strengths. (Note, however, that the analytical arguments in Sect. 2.3.4 will rely on the assumption that β is sufficiently small.)

In terms of phase-differences between neighboring oscillators ($\phi_k = \theta_{k+1} - \theta_k$), the phase model for the swimmeret neural circuit with long-range coupling is

$$\begin{aligned}
\dot{\phi_1} &= H(-\phi_1 + 0.5) + H(\phi_2) - H(\phi_1) \\
&\quad + \beta[H(\phi_2 + \phi_3) - H(\phi_1 + \phi_2)] \\
\dot{\phi_2} &= H(-\phi_2 + 0.5) + H(\phi_3) - H(-\phi_1 + 0.5) - H(\phi_2) \\
&\quad + \beta[H(-\phi_1 - \phi_2 + 0.5) - H(\phi_2 + \phi_3)] \\
\dot{\phi_3} &= H(-\phi_3 + 0.5) - H(-\phi_2 + 0.5) - H(\phi_3) \\
&\quad + \beta[H(-\phi_2 - \phi_3 + 0.5) - H(-\phi_1 - \phi_2 + 0.5)]. \quad (2)
\end{aligned}$$

Steady states of system (2) correspond to phase-locked states of the chain of HCOs (system 1).

2.3.2 Interaction functions of local modules

It is clear from the form of the phase model that the shape of the interaction function $H(\phi)$ is fundamental in determining

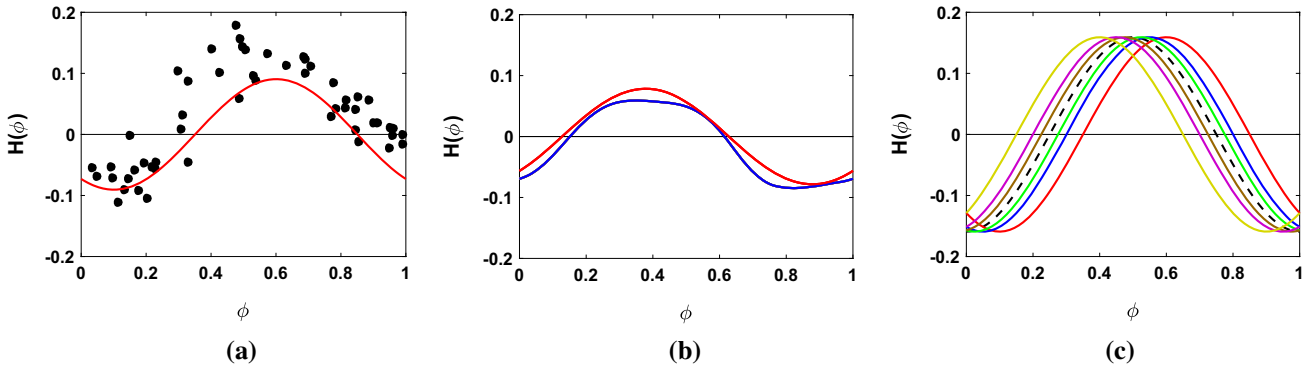

Fig. 3 Experimental, numerical, and idealized interaction functions. **a** Experimental data from this figure in Zhang et al. (2014). Data were fit to a function of the form $H(\phi) = -a\cos(2\pi(\phi+\delta))$, for $a = 0.0905$ and $\delta = -0.1007$, shown in red. The H function has a preferred phase (zero-crossing) of $\phi = 0.3507$. **b** H function generated by the Wang–Rinzel numerical simulation with a zero-crossing at $\phi = 0.1511$ (shown in blue). This H function was fit to $-a\cos(2\pi(\phi+\delta))$, for $a = 0.0784$ and $\delta = 0.1222$ (shown in red). **c** Idealized interaction function $\tilde{H}(\phi) = -\frac{1}{2\pi}\cos(2\pi\phi)$ has a zero-crossing at exactly 0.25 (dashed curve in black). In our analysis, we consider interaction functions shifted slightly away from this preferred phase, with $H(\phi) = \tilde{H}(\phi+\delta)$ for δ small. $H(\phi)$ is shown for $\delta = -0.1, -0.05, -0.025, 0.025, 0.05, 0.1$, which corresponds to red, blue, green, sienna, purple, and yellow, respectively (color figure online)

the phase-locked states of the system. Therefore, in order to understand the mechanisms underlying swimmeret coordination using the phase model, we must consider interaction functions $H(\phi)$ that capture the essential phase response properties of local modules in the crayfish swimmeret circuit.

Figure 3a depicts an experimentally measured H function for a crayfish CPG (Smarandache-Wellmann et al. 2014), and Fig. 3b shows the H function computed numerically for the Wang–Rinzel HCO model (as used in Sect. 2.2). Both of these functions are well fit by sinusoids that have zeroes with positive slope at $\phi \simeq 0.25$. The zero of an H function with positive slope is called the *preferred phase*. Previous modeling work on the crayfish swimmeret circuitry studied phase-locking in a chain of phase oscillators using sinusoidal H functions (Skinner et al. 1997). Notably, this study showed that a chain of nearest-neighbor oscillators exhibited stable 25% phase-locking when the sinusoidal interaction function was shifted to have a preferred phase at exactly $\phi = 0.25$.

In our analysis of the phase model, we represent the interaction function more generically as an arbitrary function such that $H(\phi) = \tilde{H}(\phi+\delta)$, where $\tilde{H}$ is the "unperturbed" interaction function with a preferred phase at exactly $\phi = 0.25$, i.e., where $\tilde{H}(0.25) = 0$ and $\tilde{H}'(0.25) > 0$. Provided that δ is small, H will be close to $\tilde{H}$ but the preferred phase will be shifted to $\phi = 0.25 - \delta$. This formulation allows us to evaluate the effects of small perturbations to the preferred phase of the H function.

In numerical simulations of the phase model below, we choose explicitly $\tilde{H}(\phi) = -\frac{1}{2\pi}\cos(2\pi\phi)$. The interaction function will inherent certain symmetries from this description, but our analytical results in Sect. 2.3.4 do not rely on these symmetries. In Fig. 3c, $H(\phi) = \tilde{H}(\phi+\delta)$ is plotted for various values of δ. The unperturbed $\tilde{H}(\phi)$ crosses the ϕ-axis at exactly 0.25. When $\delta > 0$, $H(\phi)$ is shifted to the left relative to $\tilde{H}(\phi)$ and $H(0.25) > 0$; for $\delta < 0$, the interaction function $H(\phi)$ is shifted to the right, which corresponds to $H(0.25) < 0$.

2.3.3 Phase model simulations of the crayfish neural circuitry

We simulate the phase model for the chain of HCOs (system (2)) and compute the phase-differences as the relative strength of the long-range coupling (β) and the shift of the interaction function (δ) vary. The results of these simulations are plotted in Fig. 4. The three frames indicate the steady-state values of ϕ_1, ϕ_2, and ϕ_3 as the long-range coupling strength β varies. Each colored curve corresponds to a different value of δ, with colors that correspond to the interaction functions shown in Fig. 3c. For small values of δ, the phases ϕ_1, ϕ_2, and ϕ_3 decrease as β increases. The H function computed for the Wang–Rinzel model has a zero close to $\phi = 0.15$ (Fig. 3b); this corresponds to the idealized sinusoidal H function with $\delta = 0.1$ (the yellow curve in Fig. 3c). Note the qualitative match between the phase-differences ϕ_1, ϕ_2 and ϕ_3 in the simulations of the chain of Wang–Rinzel HCOs (Fig. 2c) and the chain of phase oscillators with $\delta = 0.1$ (yellow curves in Fig. 4). As in the conductance-based model, the phase model simulations show that long-range connections in the crayfish neural circuitry decrease phase-differences, compared to those generated by the nearest-neighbor connectivity alone.

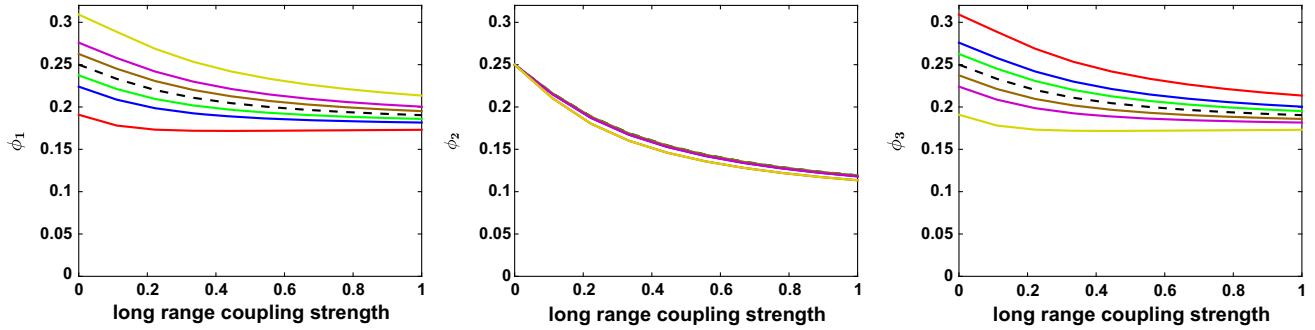

Fig. 4 The phase-locking of system (2) as δ (shift of the H function, see Fig. 3) and β, the strength of the long-range coupling vary. Steady-state values of ϕ_1 are shown in (**a**), ϕ_2 in (**b**), ϕ_3 in (**c**). Colors correspond to values of δ in Fig. 3. Steady-state values of ϕ_j tend to decrease as β increases well beyond the coupling strength's physiological range, for all j (color figure online)

2.3.4 Perturbation analysis of the phase model for the crayfish neural circuit

In this subsection, a perturbation argument is used to derive expressions that describe how the steady-state phase-differences of system (2) are modulated in response to changes in the long-range coupling strength, β, and shifts in the preferred phase of the interaction function away from 0.25, δ. In this analysis, we will assume that δ and β are sufficiently small, which are biologically reasonable assumptions. We introduce a small parameter $\epsilon << 1$ that scales δ and β, i.e., $\delta = \tilde{\delta}\epsilon$ and $\beta = \tilde{\beta}\epsilon$. (One could instead expand in the parameter δ or β and obtain identical results; however, we choose ϵ in order to explicitly retain the influence of the individual terms.) We then seek steady-state phase-differences of the form

$$\phi_j = \phi_0 + \epsilon\phi_j^* + \mathcal{O}(\epsilon^2),$$

where $\epsilon\phi_j^*$ will capture the $\mathcal{O}(\epsilon)$ modulatory effects of long-range coupling and the shifts in preferred phase.

Expanding H in terms of ϵ,

$$H(\phi_j) = \tilde{H}(\phi_j + \delta) = \tilde{H}(\phi_0) + \epsilon\tilde{H}'(\phi_0)(\phi_j^* + \tilde{\delta}) + \mathcal{O}(\epsilon^2).$$

We substitute these expressions for ϕ and H in system (2) and collect like terms of ϵ. The resulting leading order ($\mathcal{O}(1)$) steady-state equations are

$$\begin{aligned} 0 &= \tilde{H}(-\phi_0 + 0.5) \\ 0 &= -\tilde{H}(\phi_0). \end{aligned} \tag{3}$$

Note that $\phi_0 = 0.25$ always satisfies this system. Thus, the phase-differences are of the form $\phi_j = 0.25 + \epsilon\phi_j^* + \mathcal{O}(\epsilon^2)$. This phase-locked state will be stable if $\tilde{H}'(0.25) > 0$. This indicates that the system exhibits a metachronal wave with approximately 25% intersegmental phase-differences (Zhang et al. 2014). (If β is not $\mathcal{O}(\epsilon)$, $\phi_0 = 0.25$ would not be an invariant solution to the leading order equations unless $\tilde{H}(0) = \tilde{H}(0.5)$, which is not the case for experimentally measured interaction functions.)

The leading order system (3) does not include the effects of shifts of the preferred phase of the interaction function or the effects of long-range connections. To characterize the influence of these properties, we consider the $\mathcal{O}(\epsilon)$ steady-state equations for system (2)

$$\begin{aligned} 0 &= -2\phi_1^*\tilde{H}'(0.25) + \phi_2^*\tilde{H}'(0.25) + \tilde{\delta}\tilde{H}'(0.25) \\ 0 &= \phi_1^*\tilde{H}'(0.25) - 2\phi_2^*\tilde{H}'(0.25) + \phi_3^*\tilde{H}'(0.25) \\ &\quad + \tilde{\beta}(\tilde{H}(0) - \tilde{H}(0.5)) \\ 0 &= \phi_2^*\tilde{H}'(0.25) - 2\phi_3^*\tilde{H}'(0.25) - \tilde{\delta}\tilde{H}'(0.25). \end{aligned} \tag{4}$$

This set of linear equations has a solution that quantifies the $\mathcal{O}(\epsilon)$ deviation from exact 25% phase-locking

$$\begin{pmatrix} \epsilon\phi_1^* \\ \epsilon\phi_2^* \\ \epsilon\phi_3^* \end{pmatrix} = \overbrace{\frac{\delta}{2}\begin{pmatrix} 1 \\ 0 \\ -1 \end{pmatrix}}^{\text{shift term}} + \overbrace{\frac{\beta(\tilde{H}(0) - \tilde{H}(0.5))}{\tilde{H}'(0.25)}\begin{pmatrix} \frac{1}{2} \\ 1 \\ \frac{1}{2} \end{pmatrix}}^{\text{long-range coupling term}}. \tag{5}$$

The right-hand side of Eq. (5) has been decomposed into two terms: The first accounts for the effects due to the shift of the H function away from a preferred phase of 0.25, and the second term reflects the influence of long-range connections. Thus, we can consider the influence of each separately.

Deviations from exact 25% phase-differences due to shifts in the preferred phase (δ) are captured by

$$\phi_{\text{shift}}^* = \frac{\delta}{2}\begin{pmatrix} 1 \\ 0 \\ -1 \end{pmatrix}.$$

Previously, Zhang et al. studied the nearest-neighbor crayfish system in the coupled oscillator framework and showed that the system phase-locked at a state of the form $\left(0.25+\frac{H(0.25)}{2H'(0.25)}, 0.25, 0.25-\frac{H(0.25)}{2H'(0.25)}\right)$ (Zhang et al. 2014; Zhang and Lewis 2016). Our derivation reproduces that result, i.e., the expansion of the interaction function above implies that $\delta \approx \frac{H(0.25)}{H'(0.25)}$. The form of ϕ^*_{shift} highlights the asymmetric effects at the boundary of the chain of HCOs—the most anterior phase-difference differs from 0.25 by the opposite amount of the most posterior phase-difference (an amount that depends on the sign and magnitude of δ). This effect can be seen in Fig. 4. When $\beta = 0$ and δ is positive, ϕ_1 is larger than 0.25, and ϕ_3 is smaller than 0.25 by that same amount (the opposite holds when δ is negative).

Deviations from exact 25% phase-differences due to the effects of long-range coupling (β) are captured by

$$\phi^*_{\text{lr}} = \beta \frac{\tilde{H}(0) - \tilde{H}(0.5)}{\tilde{H}'(0.25)} \begin{pmatrix} \frac{1}{2} \\ 1 \\ \frac{1}{2} \end{pmatrix}.$$

If $\frac{\tilde{H}(0)-\tilde{H}(0.5)}{\tilde{H}'(0.25)} > 0$, then ϕ^*_{lr} is positive, and long-range coupling leads to increases in the phase-differences between neighboring oscillators. If $\frac{\tilde{H}(0)-\tilde{H}(0.5)}{\tilde{H}'(0.25)} < 0$, then ϕ^*_{lr} is negative, corresponding to decreases in phase-differences. Two generic properties of the interaction functions measured experimentally for the local modules in the crayfish swimmeret system and those computed for the Wang–Rinzel HCO model are that $H(0) < H(0.5)$ and $H'(0.25) > 0$ (see Fig. 3). These properties are quite robust. $H(0)$ is close to the minimum of the H function, and $H(0.5)$ near the maximum value of the H function. Furthermore, H is fairly smooth, so $H'(0.25)$ is expected to be positive. Thus, in the crayfish system, $\frac{\tilde{H}(0)-\tilde{H}(0.5)}{\tilde{H}'(0.25)} < 0$, and long-range coupling decreases the phase-differences between neighboring oscillators in a robust manner, confirming our simulation results.

3 The effect of long-range coupling during a blocked oscillator experiment

While it is difficult to directly and exclusively modulate the long-range coupling, the contribution and functional significance of these connections have been examined indirectly in experiments that blocked activity in a middle module (Tschuluun et al. 2001). These experiments eliminated nearest-neighbor inputs to either the most anterior or most posterior oscillator in the chain, leaving that oscillator to be influenced only by long-range connections. In some cases, the network retained phase-locking across this block, which provides evidence that long-range coupling can be sufficient to maintain limb coordination. In this section, we utilize our phase model to further probe the dynamics of the swimmeret neural circuit and to make predictions about the steady-state phase-locking behavior in the "blocked oscillator" experiments.

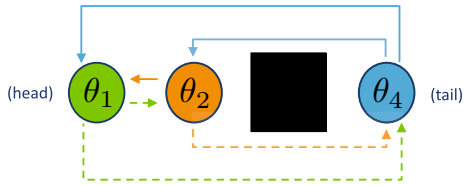

Fig. 5 Model schematic of the blocked ganglion system. The block eliminates nearest-neighbor inputs to the most posterior oscillator (θ_4), leaving it only weakly connected to the well-coupled members of the chain (θ_1 and θ_2). Dashed lines indicate the asymmetric connectivity scheme. The weak longest-range connections (between θ_1 and θ_4) are shown for biological accuracy, but their effects are not included in the analysis of the phase model

3.1 Phase model for the blocked oscillator system

To model the swimmeret neural circuit with a blocked oscillator, we eliminate all terms dependent on θ_3 in system 1 (see schematic of the system in Fig. 5),

$$\begin{aligned} \dot{\theta_1} &= \omega + H(\theta_2 - \theta_1) \\ \dot{\theta_2} &= \omega + H(\theta_1 - \theta_2 + 0.5) + \beta H(\theta_4 - \theta_2) \\ \dot{\theta_4} &= \omega + \beta H(\theta_2 - \theta_4 + 0.5). \end{aligned} \tag{6}$$

The equations governing the evolution of phase-differences between the oscillators are

$$\begin{aligned} \dot{\phi_1} &= H(-\phi_1 + 0.5) - H(\phi_1) + \beta H(\phi_{24}) \\ \dot{\phi_{24}} &= -H(-\phi_1 + 0.5) + \beta[H(-\phi_{24} + 0.5) - H(\phi_{24})], \end{aligned} \tag{7}$$

where $\phi_1 = \theta_2 - \theta_1$ and $\phi_{24} = \theta_4 - \theta_2$.

First, note that if $\beta = 0$, there is no coupling across the block, and oscillator 4 will not robustly phase-lock with oscillators 1 and 2. On the other hand, if the long-range coupling strength is increased beyond the biophysically realistic range to $\beta = 1$, the system reduces to a three-oscillator version of the nearest-neighbor configuration discussed in Sect. 2 and considered in Zhang et al. (2014) and Zhang and Lewis (2016). In that case, ϕ_{24} would approach a steady state of approximately 0.25.

This raises the following questions: What is the critical value of β (i.e., critical coupling strength) above which phase-locking exists; is this critical value in the range of experimentally measured values for next-nearest-neighbor coupling in the crayfish swimmeret system ($\beta \sim 0.3$) ; and

what are the dynamics of the system when β is close to this critical value?

3.2 Simulations of the blocked oscillator system

Simulation results of the blocked oscillator system (system (7)) are presented in Fig. 6 with each frame corresponding to a different value of β, the strength of coupling across the block. ϕ_1 is shown with a dotted black line, and ϕ_{24} is shown with a solid red line. In these simulations, $H(\phi) = -\frac{1}{2\pi}\cos(2\pi(\phi+\delta)$ with $\delta = -0.05$ (chosen arbitrarily, shown in blue in Fig. 3c).

Figure 6a shows the case where the oscillators are uncoupled across the block, $\beta = 0$. The well-coupled anterior oscillators (oscillators 1 and 2) phase-lock with a phase-difference of $\phi_1 = 0.25$. On the other hand, the oscillator uncoupled across the block (oscillator 4) is unable to coordinate its activity with the other two oscillators, and ϕ_{24} slowly "walks through" all possible phase-differences in a linear manner. Note that this phase walk-through occurs despite the fact that all of the oscillators have the same *intrinsic* frequency ω. In Fig. 6b where $\beta = 0.1$, ϕ_1 exhibits small-amplitude oscillations around 0.25. The oscillators across the block remain largely uncoordinated. As before, ϕ_{24} walks through all phases but the influence of the coupling across the block is now apparent in the nonlinear profile of ϕ_{24} in time. In Fig. 6c where $\beta = 0.2$, the dynamics are similar to those shown in Fig. 6b, but ϕ_{24} remains near 0.5 (antiphase) for an elongated period of time and the period of phase walk-through is increased. Finally, in Fig. 6d, where $\beta = 0.3$, phase-locking across the block is achieved. Note that ϕ_1 settles at a steady state very close to 0.25 ($\phi_1 = 0.258$), whereas ϕ_{24} evolves to a steady-state value of $\phi_{24} = 0.36$.

We also performed analogous simulations with $\delta > 0$ (not shown). Qualitatively similar dynamics were observed, except that in this case the phase-differences ϕ_{24} (i) decrease in time during the phase walk-throughs rather than increasing in time and (ii) exhibit prolongated activity around 0 (synchrony) instead of around 0.5 (antiphase).

3.3 Perturbation analysis of the blocked oscillator system

In order to understand the mechanisms underlying the simulation results described above, we use a perturbation argument to analyze the blocked oscillator system (system (7)) for "small" β (i.e., weak coupling across the block) and "small" δ (i.e., small shifts away from a preferred phase of 0.25) .

When long-range coupling is absent ($\beta = 0$), the system is described by

$$\dot{\phi_1} = H(-\phi_1 + 0.5) - H(\phi_1) := G(\phi_1) \quad (8)$$

$$\dot{\phi_{24}} = -H(-\phi_1 + 0.5). \quad (9)$$

Equation (8) describes the evolution of ϕ_1, the phase-difference between the coupled anterior oscillators (1 and 2). The steady-state behavior of ϕ_1 is prescribed by the zeros of $G(\phi)$. Notice that $G(0.25) = 0$, regardless of the choice of H. This occurs because the ascending and descending outputs of each oscillator are a half period out of phase with one another (see Sect. 2.3.1). Thus, $\phi_1 = 0.25$ is *always* a phase-locked state for oscillators 1 and 2. Furthermore, it is stable since $H'(0.25) > 0$. When oscillators 1 and 2 are phase-locked with $\phi_1 = 0.25$, the phase-difference across the block can be solved for explicitly as

$$\phi_{24}(t) = -H(0.25)t + \phi_{24}(0).$$

This implies that, despite all oscillators having the same *intrinsic* frequency ω, the phase-difference between oscillators 2 and 4 (ϕ_{24}) is constant only if $H(0.25) = 0$, i.e., if the preferred phase is exactly 0.25. The coupling between oscillators 1 and 2 adjusts their instantaneous frequency by $H(0.25)$ (see system (6)), introducing a frequency heterogeneity between oscillators 2 and 4. As a result, $\phi_{24}(t)$ exhibits a linear-phase walk-through in time. If $\delta < 0$, then $H(0.25) < 0$ and the phase-difference ϕ_{24} increases with time. This explains the simulation results in Fig. 6a ($\beta = 0$ and $\delta < 0$) in which $\phi_{24}(t)$ increases linearly with time. The increase is particularly slow because δ is small and $H(0.25) \simeq \tilde{H}'(0.25)\delta$. Note that if $\delta > 0$, then $H(0.25) > 0$ and the phase-difference ϕ_{24} decreases with time, whereas if $\delta = 0$, then $H(0.25) = 0$ and ϕ_{24} would remain constant at $\phi_{24}(0)$.

When long-range coupling is weak ($0 < \beta << 1$), the leading order terms in system (7) (Eqs. 8–9) dominate the dynamics of oscillators 1 and 2. Thus, ϕ_1 evolves rapidly toward and remains close to 0.25, as in the simulation results illustrated in Fig. 6. On the other hand, across the block, coordination depends on the δ-dependent size of $H(0.25)$ (i.e., $-H(-\phi_1+0.5)$ with $\phi_1 = 0.25$) relative to the β-dependent magnitude of the long-range coupling terms in system (7). For sufficiently small β and δ, the equations that govern the slow-time evolution of ϕ_{24}, as well as the small amplitude variations of ϕ_1 around 0.25, can be well approximated using the perturbation argument presented below.

As in Sect. 2.3.4, we assume that $\delta = \tilde{\delta}\epsilon$ and $\beta = \tilde{\beta}\epsilon$ with ϵ small, and we further assume that ϕ_1 has relaxed to 0.25 but allows for small ($\mathcal{O}(\epsilon)$) variations around this value,

$$\phi_1 = 0.25 + \epsilon\tilde{\phi_1}.$$

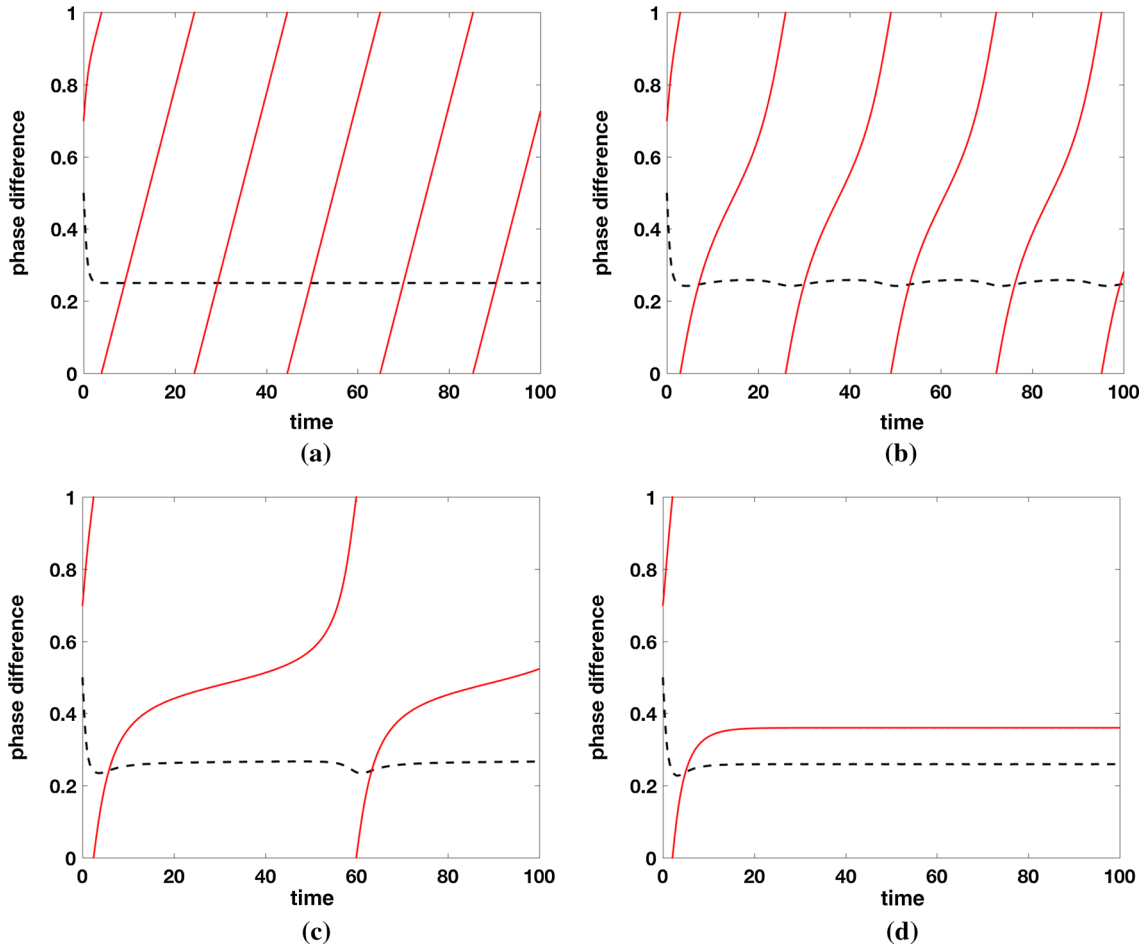

Fig. 6 Time course of phase-differences ϕ_1 (black dashed) and ϕ_{24} (red solid) with **a** $\beta = 0$, **b** $\beta = 0.1$, **c** $\beta = 0.2$, and **d** $\beta = 0.3$. In all frames, $\delta = -0.05$. **a** In the absence of long-range coupling, the phase-difference between θ_1 and θ_2 evolves to exactly 0.25, a result that holds regardless of the choice of H. The phase-difference between the uncoupled oscillators walks through all possible values. **b** For weak (nonzero) long-range coupling strengths, the well-coupled oscillators exhibit small-amplitude oscillations around 25%. The oscillators across the block exhibit a "wavy" phase walk-through. **c** As the long-range coupling strength increases, the frequency of the walk-through decreases and the phase-difference ϕ_{24} spends more time near the antiphase state, $\phi_{24} = 0.5$. **d** For sufficiently large long-range coupling strengths, system phase-locks with phase-differences close to 25% ($\phi_1 = 0.2593$ and $\phi_{24} = 0.36$) (color figure online)

Substituting this expression into the blocked oscillator model (system (7)) and expanding in ϵ, we obtain

$$\begin{aligned}\epsilon\dot{\tilde{\phi}}_1 &= H(0.25-\epsilon\tilde{\phi}_1) - H(0.25+\epsilon\tilde{\phi}_1) + \tilde{\beta}\epsilon H(\phi_{24}) \\ &= \epsilon[-2\tilde{\phi}_1(t)\tilde{H}'(0.25) + \tilde{\beta}\tilde{H}(\phi_{24})] + \mathcal{O}(\epsilon^2) \\ \dot{\phi_{24}} &= -H(0.25-\epsilon\tilde{\phi}_1(t)) + \tilde{\beta}\epsilon G(\phi_{24}) \\ &= \epsilon[(\tilde{\phi}_1(t)-\tilde{\delta})\tilde{H}'(0.25) + \tilde{\beta}\tilde{G}(\phi_{24})] + \mathcal{O}(\epsilon^2),\end{aligned}$$

where $\tilde{G}(\phi) = \tilde{H}(-\phi+0.5) - \tilde{H}(\phi)$. Here, we have assumed that $H'(0.25 \pm \phi_{24})$, $H'(0.5 \pm \phi_{24})$, and $H'(0 \pm \phi_{24})$ are $\mathcal{O}(1)$. To explicitly show that ϕ_{24} evolves on a much slower timescale than ϕ_1, we cancel the common ϵ in the first equation and rewrite the leading order equations as

$$\dot{\tilde{\phi}}_1 = [-2\tilde{\phi}_1(t)\tilde{H}'(0.25) + \tilde{\beta}\tilde{H}(\phi_{24})] \tag{10}$$

$$\dot{\phi_{24}} = \epsilon[(\tilde{\phi}_1(t)-\tilde{\delta})\tilde{H}'(0.25) + \tilde{\beta}\tilde{G}(\phi_{24})], \tag{11}$$

According to Eq. (10), $\tilde{\phi}_1$ evolves relatively rapidly to the quasi-steady state

$$\tilde{\phi}_1(t) = \frac{\tilde{\beta}\tilde{H}(\phi_{24}(t))}{2\tilde{H}'(0.25)}.$$

Substituting this expression into Eq. (11), we obtain a scalar differential equation that governs the slow-time evolution of the phase-difference between oscillators 2 and 4

$$\dot{\phi_{24}} = \epsilon\tilde{\beta}\tilde{H}'(0.25)\left(\tilde{F}(\phi_{24}) - \tilde{\delta}/\tilde{\beta}\right), \tag{12}$$

where

$$\tilde{F}(\phi_{24}) = \frac{\frac{\tilde{H}(\phi_{24})}{2} + \tilde{G}(\phi_{24})}{\tilde{H}'(0.25)}.$$

The steady-state solutions of Eq. (12), which correspond to phase-locked states between oscillator 2 and 4, must satisfy

$$\delta/\beta = \tilde{F}(\phi_{24}).$$

(The tildes on δ and β are omitted by multiplying through by the common scaling factor ϵ.) $\tilde{F}(\phi)$ is a continuous 1-periodic function with a zero at 0.25, and therefore phase-locked states will exist for δ/β sufficiently small, i.e., when the long-range coupling strength (β) is sufficiently large relative to the shift in the preferred phase of the interaction function away from 0.25 (δ). Phase-locked states at ϕ_{24} are stable when $\tilde{F}'(\phi_{24}) < 0$ and unstable when $\tilde{F}'(\phi_{24}) > 0$.

The behavior of ϕ_{24}, according to Eq. (12), is readily captured graphically by plotting $\tilde{F}(\phi)$ along with horizontal lines that correspond to various values of δ/β. Figure 7 plots an example using the interaction function $\tilde{H}(\phi) = -\frac{1}{2\pi}\cos(2\pi\phi)$ and the values of δ/β that correspond to the simulations of the blocked oscillator model shown in Fig. 6. Recall that $\delta = -0.05$ in these simulations.

(i) $\delta/\beta = -1/2$ (labeled (b) in Fig. 7) corresponds to the parameter values used in Fig. 6b ($\beta = 0.1$). In this case, $|\delta/\beta|$ is sufficiently large so that $\tilde{F}(\phi) > \delta/\beta$, i.e., $\dot{\phi}_{24}$ is always positive. Therefore, there are no phase-locked states, and ϕ_{24} will walk through all possible phases in an increasing manner, as observed in Fig. 6b.

(ii) $\delta/\beta = -1/4$ (labeled (c) in Fig. 7) corresponds to the parameter values used in Fig. 6c ($\beta = 0.2$). Again $\tilde{F}(\phi) > \delta/\beta$, and ϕ_{24} will walk through all possible phases in an increasing manner. However, in this case, δ/β is very close to, but just below, the minimum of $\tilde{F}(\phi)$, which occurs at $\phi = 0.5$, i.e., $\dot{\phi}_{24}$ is small near $\phi = 0.5$. Therefore, ϕ_{24} will remain close to 0.5 for an extended period of time during the phase walk-through, as observed in Fig. 6c.

(iii) $\delta/\beta = -1/6$ (labeled (d) in Fig. 7) corresponds to the parameter values used in Fig. 6d ($\beta = 0.3$). Here, the intersection between δ/β and $\tilde{F}(\phi)$ with $\tilde{F}'(\phi) < 0$ indicates a stable phase-locked state at $0.25 < \phi_{24} < 0.5$. Note the excellent agreement between the value of ϕ_{24} at this phase-locked state and the value from the simulation depicted in Fig. 6d (shown with a black dot).

An analogous discussion can be made for $\delta > 0$. If δ/β is sufficiently large, ϕ_{24} will exhibit phase walk-throughs that decrease with time. If δ/β is very close to, but just above, the maximum of $\tilde{F}(\phi)$, we expect phase walk-throughs that spend extended periods of time near $\phi_{24} = 0$ (synchrony), as opposed to $\phi_{24} = 0.5$ (antiphase). For sufficiently small δ/β, we expect there to be a stable phase-locked at $0 < \phi_{24} < 0.25$. Note that in the case of both $\delta > 0$ and $\delta < 0$, the phase walk-throughs of ϕ_{24} lead to oscillations of amplitude of $\mathcal{O}(\epsilon)$ in ϕ_1.

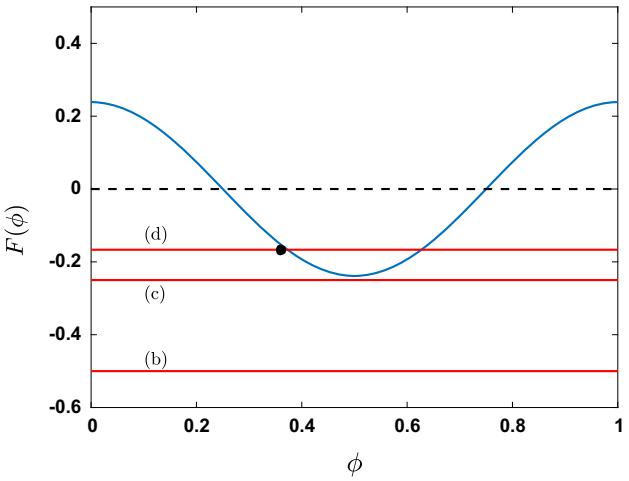

Fig. 7 Graphical representation of the dynamics of ϕ_{24}, according to Eq. 12. $\tilde{F}(\theta)$ (blue) is plotted along with three values of $\frac{\delta}{\beta}$ (red). $\delta/\beta = -0.5, -0.25$, and -0.16667 correspond to the parameter values in Fig. 6b–d, respectively. Intersections of $\tilde{F}(\theta)$ and δ/β correspond to phase-locked states with stability indicated by $\tilde{F}'(\phi)$. No phase-locking is expected for $|\delta/\beta|$ sufficiently large. The black dot indicates the value of ϕ_{24} in the phase-locked state obtained by the numerical simulation of the full blocked oscillator system with parameters corresponding to (d) (color figure online)

Figure 8 provides a more complete picture of the dependence of phase-locking across the block on long-range coupling (β) and the shift in preferred phase (δ). The values of ϕ_{24} in the phase-locked states are plotted as a function of β for two fixed values of δ (positive and negative). Red solid lines indicate stable phase-locked states, and dashed blue lines indicate unstable phase-locked states. In Fig. 8a, $\delta = -0.05$, as in Figs. 6 and 7. When β is sufficiently small, no phase-locked states exist. As β increases, a saddle-node bifurcation occurs at a critical value $\beta \sim 0.2$ with $\phi_{24} \sim 0.5$ (antiphase), giving rise to a stable and unstable phase-locked states. As β increases toward 1, the phase-difference ϕ_{24} at the stable phase-locked state decreases from ~ 0.5 toward 0.25. In Fig. 8b, $\delta = 0.1$, and a saddle-node bifurcation occurs near $\phi_{24} = 0$ (synchrony), and ϕ_{24} decreases toward 0.25 as β approaches 1.

The critical values of β and δ for phase-locking according to our perturbation analysis can be summarized in the two-parameter bifurcation diagram shown in Fig. 9. The red solid curve traces out an Arnold tongue. For values of δ and β inside this tongue, phase-locking is predicted to exist. Outside this region, phase walk-through (or higher order phase-locking) is expected. The parameter values cor-

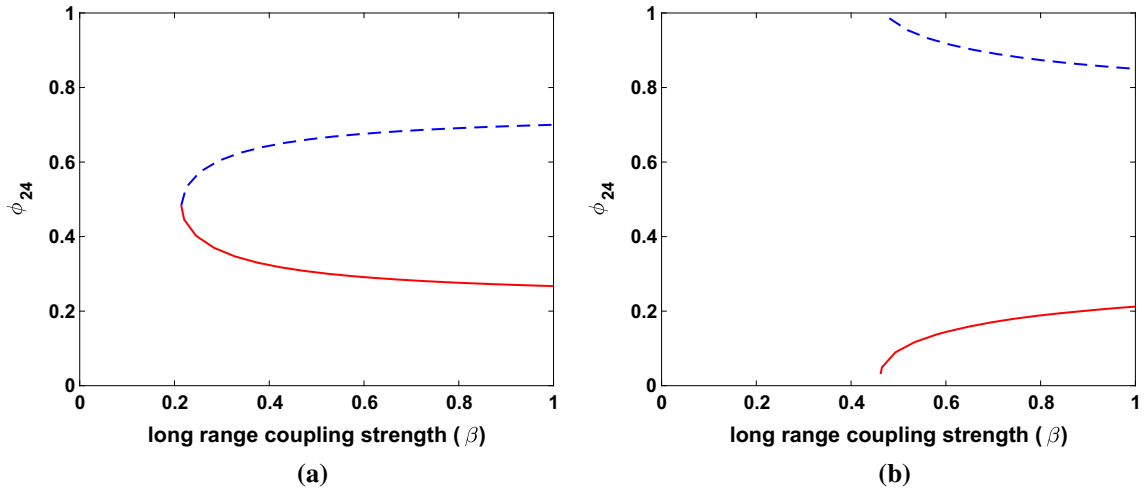

Fig. 8 Bifurcation diagrams plotting the value of ϕ_{24} in phase-locked states as the long-range coupling strength varies, for the two qualitatively different cases **a** $\delta = -0.05$ and **b** $\delta = 0.1$. Stable steady states are indicated with a red solid line; unstable steady states are indicated with a blue dotted line. In (**a**), the interaction function has a zero to the right of 0.25. There is no phase-locking for sufficiently small values of β. As β is increased, a saddle-node bifurcation occurs with ϕ_{24} close to 0.5. This corresponds to antiphase activity across the block. In (**b**), the interaction function is shifted to the left. In this case, the saddle-node bifurcation occurs with ϕ_{24} near 0, corresponding to synchrony across the block. In either case, the value of ϕ_{24} corresponding to the stable phase-locked state approaches 0.25 as β increases past the bifurcation point and beyond the physiological range of long-range coupling strengths in the intact system (color figure online)

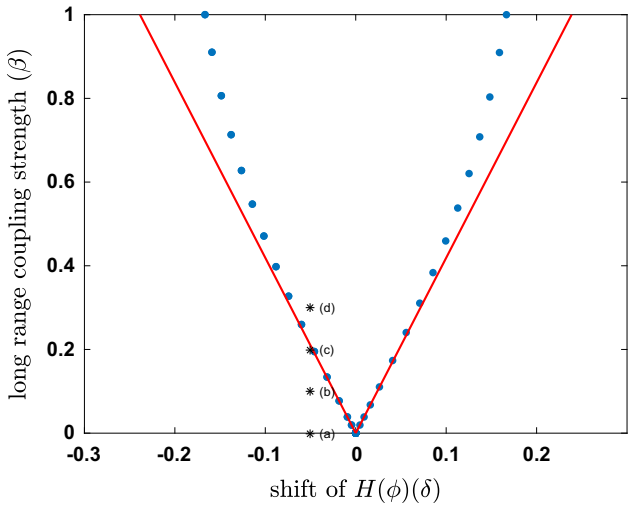

Fig. 9 Curves representing the phase-locking boundary as δ and β vary. Approximations from our perturbation argument are shown with a red lines; simulation results for the full blocked oscillator model are shown as dotted blue lines. Parameter values as in Fig. 6 are indicated (color figure online)

responding to the frames in Fig. 6a–d are indicated by dots labeled (a–d). The blue dotted curve denotes the phase-locking boundary predicted by simulations of the full blocked oscillator model. Note the good agreement between results from the perturbation analysis and the simulations, especially for $\beta < 0.5$, which includes physiological values of long-range coupling strengths.

The analysis we have presented indicates that coordination across a block depends on the ratio of the long-range coupling strength to the shift of the H function (δ/β). If this ratio is sufficiently small, our model predicts a robust phase-locked state with inter-oscillator phase-differences close to 25%. This implies that when a middle oscillator is blocked, the remaining three oscillators recover the metachronal wave with 25% inter-oscillator phase-differences. For higher values of $|\delta/\beta|$, synchrony or antiphase phase-locking across the block may be possible, but we would not expect these states to be very robust and would predict that they would be mixed with episodes of phase walk-throughs.

4 Discussion

Effective locomotion is an inherently complex behavior. The neural circuitry that drives relevant muscles and motor neurons must generate a signal that is stable and robust, yet adaptable enough to properly respond to environmental cues. Various locomotor mechanisms, including undulatory swimming in the lamprey and leech, and walking gates in the salamander (Chevallier et al. 2008), cockroach (Fuchs et al. 2011), and stick insect (Daun-Gruhn 2011) can be characterized by phase-differences between rhythmically moving limbs or body segments. For crayfish and other long-tailed crustaceans, a particular coordinated back-to-front metachronal pattern is exhibited during forward swimming, with roughly 25% phase-differences between limbs called

swimmerets. This approximately 25% delay is maintained over a wide range of frequencies and body sizes. The neural network controlling this robust behavior in the crayfish swimmeret system is comprised of a segmented chain of half-center oscillators that are all-to-all coupled, with coupling strengths that decrease with the distance of connection (Mulloney and Smarandache 2010). Previous phase models of the crayfish swimmeret circuitry have shown that the coupling topology of the nearest-neighbor connections promotes the approximately 25% phase-differences, provided that the interaction function has a zero with a positive slope near 25% (Zhang et al. 2014; Zhang and Lewis 2016). Experimentally measured interaction functions verify that this condition is met in the crayfish system (Zhang et al. 2014; Smarandache-Wellmann et al. 2014). However, these studies have simplified the coupling architecture by ignoring the presence of long-range connections. Our work explores the functional role of long-range coupling by considering how these connections influence metachronal coordination.

In this manuscript, we demonstrate that the long-range (next-nearest-neighbor) coupling in the swimmeret neural circuit decreases the phase-differences between neighboring oscillators, thus increasing the speed of the back-to-front metachronal wave of limb movement. We show this result in numerical simulations of a chain of half-center oscillators described by a conductance-based model and in a phase model—both of these models capture the essential network architecture and oscillator response properties of the swimmeret neural circuit. The decrease in phase-differences does not rely on fine tuning and persists over a wide range of long-range coupling strengths. We then make these observations rigorous using a perturbation argument in the phase model, which assumes that the long-range coupling strength is small and that the interaction function has a zero-crossing with a positive slope close to 25%. This analysis allows us to quantify the precise deviation from exact 25% phase-locking, as this deviation depends on terms which control the coupling strength and the preferred phase. When the zero-crossing is shifted away from 25%, the metachronal wave no longer exhibits uniform phase-differences. This detuning of the interaction function leads to edge effects which were previously described in Zhang et al. (2014). The long-range coupling causes additional heterogeneities in the metachronal wave state, which we now describe. The term quantifying the heterogeneity caused by the next-nearest-neighbor coupling is scaled by $H(0)-H(0.5)$. Experimentally measured interaction functions exhibit an approximately shifted sinusoidal shape where $H(0)$ is negative and $H(0.5)$ is positive. Results from Zhang and Lewis (2013) show that this appears to be a generic property of half-center oscillators. Thus, the long-range coupling affects the metachronal wave by decreasing phase-differences between limbs. Since it is highly likely that their coupling structure is similar, long-range coupling would perform the same functional role in five-limbed crustaceans like the shrimp or krill, which also exhibit approximately 25% phase-locking while swimming (see "Appendix C").

According to results from a computational fluid mechanics model of the crayfish swimmeret system, paddling with phase delays that are slightly smaller than 25% might be advantageous (Zhang et al. 2014). In this model study, uniform phase-differences between swimmerets were prescribed over a range of values from synchrony to the natural 25% and even to antiphase. Swimming efficiency peaked between 18 and 25%, suggesting that inter-limb phase-differences near but slightly less than 25% may be optimal. Thus, while the nearest-neighbor connectivity sets the phase-differences at approximately 25%, the next-nearest-neighbor connectivity may play an important functional role by decreasing the phase-differences so that they lie within a regime that is maximally efficient.

Another potential functional role of long-range coupling could be robustness to injury. Experiments show that in some cases, long-range coupling is sufficient to maintain coordination across a blocked middle oscillator (Tschuluun et al. 2001). We use a perturbation argument to detail the conditions necessary for phase-locking in this case. We again consider how coordination is influenced by the relative strength of the long-range coupling (β) and the extent to which the preferred phase of the H function is detuned (δ) away from 25%. Our analysis suggests that if the ratio δ/β is sufficiently small, the oscillators across the block would likely abandon their "normal" antiphase phase relationship and instead tend toward values closer to 25%. These predictions are corroborated by mean phase-differences computed from data presented in Tschuluun et al. (2001) (Brian Mulloney, private communication). Therefore, long-range coupling could help preserve the maximally efficient stroke pattern—a metachronal stroke with approximately 25% phase lags—even in an event where an oscillator ceases activity, especially if the long-range coupling is potentiated following injury.

We have also explored the role of longest-range (next-next-nearest-neighbor) coupling. In "Appendix B," we show that the longest-range coupling influences the phase-differences in a fundamentally different way than the long-range (next-nearest-neighbor) coupling. The connection between the most anterior and most posterior oscillators causes deviations in phase-differences that are scaled by the term $H(0.75)$. Unlike in the next-nearest-neighbor case, the sign of this term is not invariant over experimentally measured H functions, and thus a universal role for longest-range inputs cannot be concluded. The analysis does suggest, however, that this coupling generates edge effects only, similar to those caused by a detuned interaction function ($\delta \neq 0$). Thus, the longest-range coupling could either exacerbate or counteract the nonuniformity in the phase-differences caused by

this detuning. In the case of the experimental H function presented here (Fig. 3a), the latter would occur. However, since the longest-range coupling strength is quite small compared to the nearest and next-nearest-neighbor coupling strengths, and $H(0.75)/H'(0.25)$ itself is likely to be small, the influence of this term might not have significant effects on the phase-difference. Indeed, if we assume that the coupling strengths take physiologically relevant values ($\beta = 0.3$ and $\gamma = 0.1$), then the long-range coupling could vary the phase-differences on the order of 10^{-1}, but the longest-range coupling could influence the phase-differences on the order of 10^{-2} (estimated using the curve fitted to the experimental data shown in Fig. 3a).

Longer range coupling has been studied previously in generic chains of oscillators by Kopell et al. (1990). The network structure used in their study was motivated by the lamprey swimming neural circuit, which generates a metachronal wave with 1% phase delays across 100 segments. They proved that an approximate metachronal wave solution exists given certain restrictions on the H function. Under these assumptions, they showed that increasing the range of connections between oscillators tends to decrease phase-differences between neighboring oscillators. Despite the apparent similarities in some of the results in Kopell et al. to the results shown here, there are fundamental differences in the two systems. First, their work assumes that the chain of oscillators is "long," i.e., the chain of oscillators is much longer than the coupling length, and phase-locking results only apply to the interior of the chain. The chain of oscillators controlling swimmeret movement is "short," and all oscillators are connected to one another and experience boundary effects. Moreover, the H function restrictions outlined by Kopell et al. do not hold for the interaction functions we consider here, which are based on experimental data. Furthermore, while we show that the long-range coupling tends to decrease phase-differences, we also reveal that the contribution from the longest-range coupling is quite different. This coupling term contributes edge effects, which decrease the phase-difference at one end of the chain and increase the phase-difference at the other end. Thus, phase-differences between oscillators do not decrease monotonically with the number of neighboring connections between oscillators. Thus, the long-range analysis on short chains presented here is distinct from that presented by Kopell et al.

The functional implications of long-range connections have been considered in other systems. In a model of undulatory swimming in the lamprey, Cohen et al. (1992) showed that long-range coupling could alleviate the strict conditions necessary for 1% phase delays. Specifically, in nearest-neighbor oscillator models of that system, the interaction functions must be finely tuned in order to generate such small and precise phase-differences. When this model is augmented with far-reaching and sparse long-range connections and the oscillators are preferentially tuned to long-range inputs, the swimming pattern could be maintained under slight detuning. In the crayfish model, we consider H functions which are experimentally motivated, and thus the oscillators do not respond differently to neighboring and long-range connections. The crayfish system does not require such precision since the phase-differences are quite large, so a wider range of values could support phase-locking with roughly 25% delays. In fact, perturbation arguments suggest that in an intact chain, long-range inputs do not promote exact 25% differences, nor do the long-range connections tend to promote stability (see "Appendix D"). In another model, Daun-Gruhn (2011) considered long-range inputs by augmenting the known neural circuitry of the stick insect with a long-range connection that completes the circuitry as a unidirectional ring. This proposed coupling was shown to play a crucial role in the mechanism controlling switching between gaits. While the long-range coupling is not necessary for the generation of the crayfish swimming behavior, it does control features of the pattern which may ensure maximal efficiency. Collectively, these analyses suggest that long-range coupling may play an important role—either as a critical component for rhythm generation or through more subtle contributions to stability or efficiency.

Acknowledgements The authors thank Brian Mulloney for helpful discussions. This work was partially supported by the National Science Foundation under Grant CRCNS 0905063 to TJL, and Grant DMS-0931642 to LES.

Appendices

A Details of the conductance-based model

In Sect. 2.2, we describe numerical simulations of a chain of half-center oscillators (HCO) in which the dynamics of each HCO are governed by the Wang–Rinzel model. Each HCO contains a "P" and "R" neuron (see Fig. 1b). The membrane potentials and gating variables of the neurons in the jth HCO are governed by

$$\begin{aligned}
CV'_{jP} &= -g_{pir}m_\infty^3(V)h_{jP}(V_{jP}-V_{pir}) - g_L(V_{jP}-V_L)\\
&\quad - g_{Syn_I}s(V_{jR},\theta_I)(V_{jP}-V_{Syn_I})\\
h'_{jP} &= \phi[h_\infty(V_{jP}) - h_{jP}]/\tau_h(V_{jP})\\
CV'_{jR} &= -g_{pir}m_\infty^3(V)h_{jR}V_{jR}-V_{pir}) - g_L(V_{jR}-V_L)\\
&\quad - g_{Syn_I}s(V_{iP},\theta_I)(V_{iR}-V_{Syn_I})\\
&\quad - \sum_{i\in exc(j)} g_{Syn_E}s(V_i,\theta_E)(V_{jR}-V_{Syn_E})\\
h'_{jR} &= \phi[h_\infty(V_{jR}) - h_j]/\tau_h(V_{jR})
\end{aligned}$$

with $j \in \{1,2,3,4\}$ and $m_\infty(V) = \frac{1}{1+e^{(V+65)/7.8}}$, $h_\infty(V) = \frac{1}{1+e^{(V+81)/11}}$, $\tau_h(V) = h_\infty(V)e^{(V+162.3)/17.8}$, and $s(V,\theta) = \frac{1}{1+e^{-(V-\theta)/k_{Syn}}}$ (Wang and Rinzel 1992). The excitatory inputs to neuron jR are indexed by $exc(j)$, respectively, and correspond to the schematic shown in Fig. 1b. Parameters were adapted from (Wang and Rinzel 1992): $C = 1\,\mu\text{F/cm}^2$, $V_{pir} = 120\,\text{mV}$, $g_L = 0.1\,\text{mS/cm}^2$, $V_L = -60\,\text{mV}$, $V_{SynI} = -80\,\text{mV}$, $\phi = 3$, $V_{SynE} = 0\,\text{mV}$, $g_{Syn_I} = 0.2\,\text{mS/cm}^2$, $g_{Syn_E} = 0.03 \cdot g_{Syn_I}\,\text{mS/cm}^2$, $\theta_I = -44\,\text{mV}$, $k_{Syn} = 2\,\text{mV}$, $\theta_E = -56\,\text{mV}$, $g_{PiR} = 0.3\,\text{mS/cm}^2$.

B The effects of the longest-range connections

Here, we consider the effects from the connections between the most posterior and the most anterior oscillators, i.e., the coupling between next-next-nearest-neighbors.

B.1 Phase model of the complete neural circuitry

We augment the phase model (system (1)) with connections between oscillators 1 and 4 to obtain

$$\begin{aligned}
\dot{\theta_1} &= \omega + H_A(\theta_2-\theta_1) + \beta H_A(\theta_3-\theta_1) + \gamma H_A(\theta_4-\theta_1)\\
\dot{\theta_2} &= \omega + H_D(\theta_1-\theta_2) + H_A(\theta_3-\theta_2) + \beta H_A(\theta_4-\theta_2)\\
\dot{\theta_3} &= \omega + H_D(\theta_2-\theta_3) + H_A(\theta_4-\theta_3) + \beta H_D(\theta_1-\theta_3)\\
\dot{\theta_4} &= \omega + H_D(\theta_3-\theta_4) + \beta H_D(\theta_2-\theta_4) + \gamma H_D(\theta_1-\theta_4).
\end{aligned} \tag{13}$$

Similar to the parameter β that scales the long-range (next-nearest-neighbor) connections, we scale the longest-range connections by the parameter γ. Recall that the long-range coupling strength (β) has been shown in experiments to be roughly 30% of the strength between nearest-neighbors, and the longest-range coupling strength (γ) has been shown to be roughly 10% of the strength between neighbors.

By incorporating the topology of the connections into our model as we did in Sect. 2.3.1, we obtain an analogous system that governs the evolution of phase-differences between neighboring HCOs

$$\begin{aligned}
\dot{\phi_1} &= H(-\phi_1+0.5) + H(\phi_2) - H(\phi_1)\\
&\quad + \beta[H(\phi_2+\phi_3) - H(\phi_1+\phi_2)] - \gamma H(\phi_1+\phi_2+\phi_3)\\
\dot{\phi_2} &= H(-\phi_2+0.5) + H(\phi_3) - H(-\phi_1+0.5) - H(\phi_2)\\
&\quad + \beta[H(-\phi_1-\phi_2+0.5) - H(\phi_2+\phi_3)]\\
\dot{\phi_3} &= H(-\phi_3+0.5) - H(-\phi_2+0.5) - H(\phi_3)\\
&\quad + \beta[H(-\phi_2-\phi_3+0.5) - H(-\phi_1-\phi_2+0.5)]\\
&\quad + \gamma H(-\phi_1-\phi_2-\phi_3+0.5).
\end{aligned} \tag{14}$$

B.2 The influence of "longest-range" coupling is different than the influence of next-nearest-neighbor coupling

We perform a perturbation analysis as in Sect. 2.3.4, and look for steady-state phase-differences for system (14) of the form

$$\phi_j = \phi_0 + \epsilon\phi_j^* + \mathcal{O}(\epsilon^2).$$

As before, we assume that ϵ scales the shift term δ, the long-range coupling strength β, and now the longest-range coupling strength γ, i.e., $\gamma = \tilde{\gamma}\epsilon$. With these assumptions, the leading order equations for system (14) remain system (3), and therefore, $\phi_j = 0.25 + \epsilon\phi_j^* + \mathcal{O}(\epsilon^2)$. Including the longest-range connections augments the $\mathcal{O}(\epsilon)$ system with two additional γ dependent terms

$$\begin{aligned}
0 &= -2\phi_1^*\tilde{H}'(0.25) + \phi_2^*\tilde{H}'(0.25) + \tilde{\delta}\tilde{H}'(0.25) - \tilde{\gamma}\tilde{H}(0.75)\\
0 &= \phi_1^*\tilde{H}'(0.25) - 2\phi_2^*\tilde{H}'(0.25) + \phi_3^*\tilde{H}'(0.25) + \tilde{\beta}(\tilde{H}(0) - \tilde{H}(0.5))\\
0 &= \phi_2^*\tilde{H}'(0.25) - 2\phi_3^*\tilde{H}'(0.25) - \tilde{\delta}\tilde{H}'(0.25) + \tilde{\gamma}\tilde{H}(0.75).
\end{aligned}$$

The ϕ_j^* now satisfy the linear system

$$\begin{pmatrix} -2 & 1 & 0\\ 1 & -2 & 1\\ 0 & 1 & -2 \end{pmatrix}\begin{pmatrix}\phi_1^*\\ \phi_2^*\\ \phi_3^*\end{pmatrix} = \overbrace{\tilde{\delta}\begin{pmatrix}-1\\0\\1\end{pmatrix}}^{\text{shift term}} + \overbrace{\frac{\tilde{\beta}}{\tilde{H}'(0.25)}\begin{pmatrix}0\\ \tilde{H}(0.5)-\tilde{H}(0)\\0\end{pmatrix}}^{\text{long-range coupling term}} + \overbrace{\frac{\tilde{\gamma}\tilde{H}(0.75)}{\tilde{H}'(0.25)}\begin{pmatrix}1\\0\\-1\end{pmatrix}}^{\text{longest-range coupling}},$$

which implies

$$\begin{pmatrix}\epsilon\phi_1^*\\ \epsilon\phi_2^*\\ \epsilon\phi_3^*\end{pmatrix} = \overbrace{\frac{\delta}{2}\begin{pmatrix}1\\0\\-1\end{pmatrix}}^{\text{shift term}} + \overbrace{\frac{\beta(\tilde{H}(0)-\tilde{H}(0.5))}{\tilde{H}'(0.25)}\begin{pmatrix}\frac{1}{2}\\1\\\frac{1}{2}\end{pmatrix}}^{\text{long-range coupling term}} + \overbrace{\frac{\gamma\tilde{H}(0.75)}{2\tilde{H}'(0.25)}\begin{pmatrix}-1\\0\\1\end{pmatrix}}^{\text{longest-range coupling}}.$$

This equation is identical to Eq. (5), except for an additional term that quantifies the effects of the longest-range coupling

$$\phi_{\text{llr}}^* = \gamma\frac{\tilde{H}(0.75)}{2\tilde{H}'(0.25)}\begin{pmatrix}-1\\0\\1\end{pmatrix}.$$

The longest-range coupling modulates the most anterior and posterior phase-differences by equal but opposite amounts. The direction of the modulation depends on the sign of the

interaction function at 0.75. Note that for the HCOs under consideration, $\tilde{H}'(0.25) > 0$. The longest-range (γ) term and the H function shift (δ) term have similar formulas but differ only by a scalar multiple; thus, the long-range coupling could either exacerbate the edge effects due to the shift of the H function, or counteract them. For all of the H functions we consider here, including the experimentally measured H function in Fig. 3a, the γ term exacerbates the edge effects caused by the δ term, leading to an increased gradient in phase-differences between oscillators.

C Next-nearest-neighbor connections in longer chains

Along with the crayfish, some five-limbed crustaceans exhibit the approximately 25% phase lag during forward swimming; therefore, we extend our analysis to consider longer finite chains of HCOs with nearest-neighbor and next-nearest-neighbor coupling. We show that for an asymmetrically coupled chain of arbitrary length, next-nearest coupling tends to decrease phase-difference between oscillators. For a chain of arbitrary length $n \geq 5$,

$$\begin{aligned}
\dot{\theta}_1 &= \omega + H_A(\theta_2 - \theta_1) + \beta H_A(\theta_3 - \theta_1)\\
&= \omega + H(\phi_1) + \beta H(\phi_1 + \phi_2)\\
\dot{\theta}_2 &= \omega + H(\phi_1) + \beta H(\phi_1 + \phi_2)\\
&= \omega + H(-\phi_1 + 0.5) + H(\phi_2) + \beta H(\phi_2 + \phi_3)\\
\dot{\theta}_k &= \omega + H_D(\theta_{k-1} - \theta_k) + H_A(\theta_{k+1} - \theta_k)\\
&\quad + \beta H_D(\theta_{k-2} - \theta_k) + \beta H_A(\theta_{k+2} - \theta_k)\\
&= \omega + H(-\phi_{k-1} + 0.5) + H(\phi_k)\\
&\quad + \beta H(-\phi_{k-2} - \phi_{k-1} + 0.5) + \beta H(\phi_k + \phi_{k+1})\\
\dot{\theta}_{n-1} &= \omega + H_D(\theta_{n-2} - \theta_{n-1}) + H_A(\theta_n - \theta_{n-1})\\
&\quad + \beta H_D(\theta_{n-3} - \theta_{n-1})\\
&= \omega + H(-\phi_{n-2} + 0.5) + H(\phi_{n-1})\\
&\quad + \beta H(-\phi_{n-2} - \phi_{n-3} + 0.5)\\
\dot{\theta}_n &= \omega + H_D(\theta_{n-1} - \theta_n) + \beta H_D(\theta_{n-2} - \theta_n)\\
&= \omega + H(-\phi_{n-1} + 0.5) + \beta H(-\phi_{n-2} - \phi_{n-1} + 0.5)
\end{aligned}$$

This gives us the system of phase-differences

$$\begin{aligned}
\dot{\phi}_1 &= H(-\phi_1 + 0.5) + H(\phi_2) - H(\phi_1)\\
&\quad + \beta H(\phi_2 + \phi_3) - \beta H(\phi_1 + \phi_2)\\
\dot{\phi}_2 &= H(-\phi_2 + 0.5) + H(\phi_3) - H(-\phi_1 + 0.5)\\
&\quad - H(\phi_2) + \beta H(-\phi_1 - \phi_2 + 0.5)\\
&\quad + \beta H(\phi_3 + \phi_4) - \beta H(\phi_2 + \phi_3)\\
\dot{\phi}_k &= H(-\phi_k + 0.5) + H(\phi_{k+1})\\
&\quad - H(-\phi_{k-1} + 0.5) - H(\phi_k)\\
&\quad + \beta H(-\phi_{k-1} - \phi_k + 0.5) + \beta H(\phi_{k+1} + \phi_{k+2})\\
&\quad - \beta H(-\phi_{k-2} - \phi_{k-1} + 0.5) - \beta H(\phi_k + \phi_{k+1})\\
\dot{\phi}_{n-2} &= H(-\phi_{n-2} + 0.5) + H(\phi_{n-1}) - H(-\phi_{n-3} + 0.5)\\
&\quad - H(\phi_{n-2}) + \beta H(-\phi_{n-2} - \phi_{n-3} + 0.5)\\
&\quad - \beta H(-\phi_{n-4} - \phi_{n-3} + 0.5) - \beta H(\phi_{n-2} + \phi_{n-1})\\
\dot{\phi}_{n-1} &= H(-\phi_{n-1} + 0.5) - H(-\phi_{n-2} + 0.5)\\
&\quad - H(\phi_{n-1}) + \beta H(-\phi_{n-2} - \phi_{n-1} + 0.5)\\
&\quad - \beta H(-\phi_{n-2} - \phi_{n-3} + 0.5)
\end{aligned}$$

Using a perturbation argument with assumptions as in the main text, the $\mathcal{O}(1)$ system yields $\phi_0 = 0.25$. Here, the contribution from the long-range coupling satisfies

$$A\phi^*_{\mathrm{lr}} = \frac{\tilde{\beta}}{\tilde{H}'(0.25)} \begin{pmatrix} 0 \\ -\tilde{H}(0) \\ 0 \\ \cdots \\ 0 \\ \tilde{H}(0.5) \\ 0 \end{pmatrix}$$

where A is an $(n-1)$ by $(n-1)$ tridiagonal Topelitz matrix, with -2 on the main diagonal and ones along the off diagonals. Independent of n, the inverse of this matrix has all nonpositive components, causing $\phi^*_{\mathrm{lr}} \leq 0$, as claimed.

D Effects of long-range coupling on stability of phase-locking

The 25% phase-locked state in the phase model of the chain of HCOs (system (2)) inherits its stability from the leading order system in which there are no effects of long-range coupling ($\beta = \epsilon\tilde{\beta} = 0$) and the preferred phase is 0.25 ($\delta = \epsilon\tilde{\delta} = 0$). That is, it is stable if $\tilde{H}'(0.25)$. Here, we assess the modulatory influence of long-range coupling and shifts in preferred phase on the stability of the $\sim$ 25% phase-locked state by determining their $\mathcal{O}(\epsilon)$ effects on the eigenvalues of the system linearized around the phase-locked state.

By computing the Jacobian of the system, evaluating it at $\phi_k = 0.25$, and substituting in the solution form found in Eq. 5, we obtain (to $\mathcal{O}(\epsilon)$)

$$\begin{aligned}
J &= J_0 + \epsilon J_1\\
&= \tilde{H}'(0.25) \begin{pmatrix} -2 & 1 & 0 \\ 1 & -2 & 1 \\ 0 & 1 & -2 \end{pmatrix}\\
&\quad + \tilde{\delta}\epsilon\tilde{H}''(0.25) \begin{pmatrix} -2 & 1 & 0 \\ \frac{1}{2} & -2 & \frac{1}{2} \\ 0 & 1 & -2 \end{pmatrix}
\end{aligned}$$

$$+\tilde{\beta}\epsilon\frac{\tilde{H}(0)-\tilde{H}(0.5)}{\tilde{H}'(0.25)}\tilde{H}''(0.25)\begin{pmatrix}0&1&0\\-\frac{1}{2}&0&\frac{1}{2}\\0&-1&0\end{pmatrix}$$
$$+\tilde{\beta}\epsilon\tilde{H}'(0.5)\begin{pmatrix}-1&0&1\\0&-1&-1\\0&0&0\end{pmatrix}$$
$$+\tilde{\beta}\epsilon\tilde{H}'(0)\begin{pmatrix}0&0&0\\-1&-1&0\\1&0&-1\end{pmatrix}$$

We seek the eigenvalues λ of this Jacobian, that is $J\Phi=\lambda\Phi$. We take the eigenvalues and eigenvectors of J to be of the form $\lambda=\lambda_0+\epsilon\lambda_1$ and $\Phi=\Phi_0+\epsilon\Phi_1$ and note that $\lambda_1=<J_1\Phi_0,\Phi_0>$. Assuming that $\tilde{H}'(0.25)$, the eigenvalues of J_0 are all negative. Therefore, to assess stability of the $\sim$ 25% phase-locked state, we need only consider the smallest eigenvalue, which is $\lambda_0=\tilde{H}'(0.25)(-2+\sqrt{2})$ and has a corresponding eigenvector $\Phi_0=-\frac{1}{2}(1,\sqrt{2},1)^{\mathrm{T}}$. A simple calculation shows that

$$\lambda_1=\tilde{\delta}\tilde{H}''(0.25)\frac{-8+3\sqrt{2}}{4}+\tilde{\beta}(\tilde{H}'(0.5)+\tilde{H}'(0))\frac{-2-\sqrt{2}}{4}.$$

Both of the numerical fractions take values close to -1. Furthermore, for the idealized interaction functions that we have considered here, $\tilde{H}''(0.25)$, $\tilde{H}'(0.5)$, and $\tilde{H}'(0)$ are small. This implies that long-range coupling and shifts in preferred phase have negligible ($\mathcal{O}(\epsilon^2)$) effects on stability.

References

Chevallier S, Ijspeert AJ, Ryczko D, Nagy F, Cabelguen JM (2008) Organisation of the spinal central pattern generators for locomotion in the salamander: biology and modelling. Brain Res Rev 57(1):147–161

Cohen AH, Ermentrout GB, Kiemel T, Kopell N, Sigvardt KA, Williams TL (1992) Modelling of intersegmental coordination in the lamprey central pattern generator for locomotion. Trends Neurosci 15(11):434–438

Daun-Gruhn S (2011) A mathematical modeling study of intersegmental coordination during stick insect walking. J Comput Neurosci 30(2):255–278

Fuchs E, Holmes P, Kiemel T, Ayali A (2011) Intersegmental coordination of cockroach locomotion: adaptive control of centrally coupled pattern generator circuits. Front Neural Circuits 4:125

Hughes G, Wiersma C (1960) The co-ordination of swimmeret movements in the crayfish, *Procambarus clarkii* (Girard). J Exp Biol 37(4):657–670

Jones S, Kopell N (2006) Local network parameters can affect inter-network phase lags in central pattern generators. J Math Biol 52(1):115–140

Jones SR, Mulloney B, Kaper TJ, Kopell N (2003) Coordination of cellular pattern-generating circuits that control limb movements: the sources of stable differences in intersegmental phases. J Neurosci 23(8):3457–3468

Kopell N, Zhang W, Ermentrout G (1990) Multiple coupling in chains of oscillators. SIAM J Math Anal 21(4):935–953

Laverack M, Macmillan D, Neil D (1976) A comparison of beating parameters in larval and post-larval locomotor systems of the lobster *Homarus gammarus* (L.). Philos Trans R Soc B Biol Sci 274(929):87–99

Marder E, Bucher D (2001) Central pattern generators and the control of rhythmic movements. Curr Biol 11(23):R986–R996

Mulloney B (1997) A test of the excitability-gradient hypothesis in the swimmeret system of crayfish. J Neurosci 17(5):1860–1868

Mulloney B, Smarandache C (2010) Fifty years of CPGs: two neuroethological papers that shaped the course of neuroscience. Front Behav Neurosci 4:45

Mulloney B, Smarandache-Wellmann C (2012) Neurobiology of the crustacean swimmeret system. Prog Neurobiol 96(2):242–267

Mulloney B, Harness PI, Hall WM (2006) Bursts of information: coordinating interneurons encode multiple parameters of a periodic motor pattern. J Neurophysiol 95(2):850–861

Paul DH, Mulloney B (1986) Intersegmental coordination of swimmeret rhythms in isolated nerve cords of crayfish. J Comp Physiol A 158(2):215–224

Perkel DH, Mulloney B (1974) Motor pattern production in reciprocally inhibitory neurons exhibiting postinhibitory rebound. Science 185(4146):181–183

Schwemmer M, Lewis TJ (2012) The theory of weakly coupled oscillators. PRCs Neurosci Theory Exp Anal 6:3–31

Skinner FK, Kopell N, Mulloney B (1997) How does the crayfish swimmeret system work? Insights from nearest-neighbor coupled oscillator models. J Comput Neurosci 4(2):151–160

Smarandache C, Hall WM, Mulloney B (2009) Coordination of rhythmic motor activity by gradients of synaptic strength in a neural circuit that couples modular neural oscillators. J Neurosci 29(29):9351–9360

Smarandache-Wellmann C, Grätsch S (2014) Mechanisms of coordination in distributed neural circuits: encoding coordinating information. J Neurosci 34(16):5627–5639

Smarandache-Wellmann C, Weller C, Wright TM, Mulloney B (2013) Five types of nonspiking interneurons in local pattern-generating circuits of the crayfish swimmeret system. J Neurophysiol 110(2):344–357

Smarandache-Wellmann C, Weller C, Mulloney B (2014) Mechanisms of coordination in distributed neural circuits: decoding and integration of coordinating information. J Neurosci 34(3):793–803

Somers D, Kopell N (1993) Rapid synchronization through fast threshold modulation. Biol Cybern 68(5):393–407

Tschuluun N, Hall WM, Mulloney B (2001) Limb movements during locomotion: tests of a model of an intersegmental coordinating circuit. J Neurosci 21(19):7859–7869

Wang XJ, Rinzel J (1992) Alternating and synchronous rhythms in reciprocally inhibitory model neurons. Neural Comput 4(1):84–97

Williams TL, Sigvardt KA, Kopell N, Ermentrout GB, Remler MP (1990) Forcing of coupled nonlinear oscillators: studies of intersegmental coordination in the lamprey locomotor central pattern generator. J Neurophysiol 64(3):862–871

Zhang C, Lewis TJ (2013) Phase response properties of half-center oscillators. J Comput Neurosci 35(1):55–74

Zhang C, Lewis TJ (2016) Robust phase-waves in chains of half-center oscillators. J Math Biol 74(7):1627–1656

Zhang C, Guy RD, Mulloney B, Zhang Q, Lewis TJ (2014) Neural mechanism of optimal limb coordination in crustacean swimming. Proc Natl Acad Sci 111(38):13840–13845